



Dynamics of “jumping” Trojans: a perturbative treatment

Vladislav V. Sidorenko^{1,2}

Received: 29 November 2017 / Revised: 30 August 2018 / Accepted: 5 September 2018 /

Published online: 5 October 2018

© Springer Nature B.V. 2018

Abstract

The term “jumping” Trojan was introduced by Tsiganis et al. (Astron Astrophys 354:1091–1100, 2000) in their studies of long-term dynamics exhibited by the asteroid (1868) Thersites, which had been observed to jump from librations around L_4 to librations around L_5 . Another example of a “jumping” Trojan was found by Connors et al. (Nature 475:481–483, 2011): librations of the asteroid 2010 TK7 around the Earth’s libration point L_4 preceded by its librations around L_5 . We explore the dynamics of “jumping” Trojans under the scope of the restricted planar elliptical three-body problem. Via double numerical averaging we construct evolutionary equations, which allow analyzing transitions between *different regimes of orbital motion*.

Keywords Restricted three-body problem · Trojan asteroids · Secular evolution

1 Introduction

An asteroid at 1:1 mean motion resonance with one of the main planets most often moves either in a “tadpole” orbit (T -orbit) or in a “horseshoe” orbit (HS-orbit). T -orbits cycle around one of the triangular libration points, whereas HS-orbits encompass both triangular libration points as well as the collinear libration point L_3 . Other types of resonant co-orbital motion—in particular, quasi-satellite (QS) regimes or compound QS + HS orbits—are also possible, although they are less common. The formal difference between these orbits is the behavior of the resonance phase $\varphi = \lambda - \lambda'$, where λ and λ' are the mean longitudes of the asteroid and the planet, respectively (Namouni et al. 1999).

If several modes of motion are possible for a Hamiltonian system at resonance, then under certain conditions the transitions between these modes can be observed. It was shown in

This article is part of the topical collection on Recent advances in the study of the dynamics of N-body problem.

Guest Editors: Giovanni Federico Gronchi, Ugo Locatelli, Giuseppe Pucacco and Alessandra Celletti.

✉ Vladislav V. Sidorenko
vvsidorenko@list.ru

¹ Keldysh Institute of Applied Mathematics, Russian Academy of Sciences, Miusskaya Sq., 4, Moscow, Russia 125047

² Moscow Institute of Physics and Technology, Institutskiy S-Str., 9, Dolgoprudny, Russia 141700

Tsiganis et al. (2000) that Trojan asteroid (1868) Thersites will make a $T_L \rightarrow T_T$ transition (T_L and T_T denote T -orbits enclosing the “leading” and the “trailing” libration points L_4 and L_5 , respectively). Numerical integration also indicates that the asteroid 2010TK7 (the first Trojan asteroid of the Earth) makes transitions between the motions in the neighborhood of L_4 and L_5 (Connors et al. 2011; Dvorak et al. 2012). Further examples of similar “jumps” in the dynamics of real Trojans were discussed by de la Fuente Marcos and de la Fuente Marcos (2012), Schwarz and Dvorak (2012) and Galliazzo and Schwarz (2014).

Secular evolution of Trojan asteroids has been a point of interest for many specialists. A detailed bibliography can be found in Erdi (1997), Marzari et al. (2002) and Robutel and Souchay (2010). The necessity to investigate the Trojans’ jumps in simplified dynamical models was emphasized by Schwarz and Dvorak (2012). For the time being, it seems that only Oshima and Yanao (2015) attempted an analytical study of the transitions

$$T_L \rightarrow T_T, \quad T_T \rightarrow T_L, \quad T_{L,T} \rightarrow \text{HS}, \quad \text{HS} \rightarrow T_{L,T}. \quad (1)$$

Their analysis was based mainly on the consideration of the planar restricted circular three-body problem. Oshima and Yanao ascribe the motions with transitions (1) to the region of chaotic dynamics generated by the intersection of stable and unstable manifolds of periodic solutions encircling the libration point L_3 . However, the interpretation of transitions (1) as a certain homoclinic phenomenon has a serious drawback—the measure of the initial conditions giving rise to motions with transitions (1) turns out to be very small ($\sim \exp(-C/\sqrt{\mu})$, where μ characterizes the relative part of the planet’s mass in the total mass of the system “Sun + planet,” $C = \text{const} > 0$; the presented estimate follows from some general results, obtained by Neishtadt (1984).

We aim to demonstrate that in the context of the planar-restricted elliptic three-body problem “Sun + planet + asteroid” there is another mechanism underlying the transitions (1). To reveal this mechanism, we apply the basic ideas of the approach proposed by Wisdom to study the transformations of the resonance motions (Wisdom 1985). It also allows establishing dynamical robustness of the discussed transitions in the elliptic problem—they occur for the set of initial conditions, whose measure does not depend on μ . The core object in this approach is an auxiliary 1DOF Hamiltonian system, which governs the variation of the resonance phase φ . Quantities that characterize the shape and the orientation of asteroid’s osculating orbit are interpreted as slowly varying parameters whose change leads to qualitative transformations in the behavior of φ . Previously such an approach was used to study the transitions between different regimes of co-orbital motion in Namouni et al. (1999), Nesvorný et al. (2002) and Sidorenko et al. (2014).

We hope our analysis to become a useful addition to the prior research on the secular effects in the dynamics of Trojan asteroids on the basis of the modern theory of resonance phenomena in Hamiltonian systems (Beaugè and Roig 2001; Morais 2001). Of course, the consideration of the three-body problem does not explain the transition $T_L \rightarrow T_T$, demonstrated by the asteroid (1868) Thersites—the numerical results presented by Tsiganis et al. (2000) indicate a significant influence of secular resonances on the dynamics of this asteroid. The mechanism of transitions that we are discussing is probably realized in the dynamics of the so-called temporary Trojans (Karlsson 2004). Since their stay in certain regimes of motion is relatively short, the effects due to secular resonances can be neglected.

2 Averaged motion equations for studying the dynamics of the asteroid at 1:1 mean motion resonance

2.1 Averaging over orbital motion

We assume that the planet’s orbit around the star to have an eccentricity e' , semimajor axis of unit length, and the sum of masses of the star and the planet to make the unit mass. The unit time is chosen so that the orbital period of the planet equals 2π . The mass of the planet μ is substantially smaller than that of the star and is further treated as a small parameter. The motion of the asteroid is restricted to the plane of the primaries’ motion (i.e., we consider the planar problem).

Following general recommendations on analysis of the resonance phenomena (e.g., Arnold et al. 2006), we focus our attention on the region \mathcal{Z}_{res} of the system’s phase space, defined by the condition

$$|n - n'| \lesssim \mu^{1/2}.$$

Here n and $n' = 1$ are the mean motions of the asteroid and the planet, respectively. The phase variables are

$$x, y, L, \varphi,$$

where x, y , and L are the Poincaré elements, which are related to osculating elements by the formulae

$$\begin{aligned} x &= \sqrt{2\sqrt{(1-\mu)a} \left[1 - \sqrt{(1-e^2)} \right]} \cos \varpi, \\ y &= -\sqrt{2\sqrt{(1-\mu)a} \left[1 - \sqrt{(1-e^2)} \right]} \sin \varpi, \\ L &= \sqrt{(1-\mu)a}. \end{aligned} \tag{2}$$

Here ϖ, e , and a , are the longitude of the periapsis, the eccentricity, and the semimajor axis of the asteroid orbit, respectively.

The equations of motion have the canonical form

$$\begin{aligned} \frac{dx}{dt} &= -\frac{\partial \mathcal{K}}{\partial y}, & \frac{dy}{dt} &= \frac{\partial \mathcal{K}}{\partial x}, \\ \frac{dL}{dt} &= -\frac{\partial \mathcal{K}}{\partial \varphi}, & \frac{d\varphi}{dt} &= \frac{\partial \mathcal{K}}{\partial L}, \end{aligned} \tag{3}$$

with the Hamiltonian

$$\mathcal{K} = -\frac{(1-\mu)^2}{2L^2} - L - \mu \mathcal{R}. \tag{4}$$

The disturbing function \mathcal{R} in the expression for \mathcal{K} is defined as

$$\mathcal{R} = \frac{1}{|\mathbf{r} - \mathbf{r}'|} - \frac{(\mathbf{r}, \mathbf{r}')}{r'^3},$$

where $\mathbf{r} = \mathbf{r}(x, y, L, \lambda(\varphi, \lambda'))$ and $\mathbf{r}' = \mathbf{r}'(\lambda')$ are the position vectors of the asteroid and the planet relative to the star.

Averaging of (3) over the orbital motion of the asteroid and the planet is equivalent to substituting the function

$$W(x, y, L, \varphi) = \frac{1}{2\pi} \int_0^{2\pi} R(x, y, L, \lambda(\lambda', \varphi), \lambda') d\lambda' \tag{5}$$

instead of the function \mathcal{R} in the expression (4) for \mathcal{K} .

Such averaging eliminates the mean longitude of the planet $\lambda' = t + \lambda'_0$ from the right-hand sides of the equations of motion. Therefore, these equations become autonomous.

In our study, the averaging (5) is carried out numerically. Technically, this is similar to the averaging of the disturbing function at 3:1 MMR described in detail in Sidorenko (2006). Let us note that numerical averaging of a disturbing function at MMR is a common technique (e.g., Schubart 1964).

2.2 The “slow-fast” system

We shall now proceed with the scale transformation

$$\tau = \sqrt{\mu}t, \quad \Phi = (1 - L)/\sqrt{\mu}.$$

Without loss of accuracy the averaged equations of motion in the resonance zone \mathcal{Z}_{res} can be rewritten as follows:

$$\begin{aligned} \frac{d\varphi}{d\tau} &= 3\Phi, & \frac{d\Phi}{d\tau} &= -\frac{\partial V}{\partial \varphi}, \\ \frac{dx}{d\tau} &= \varepsilon \frac{\partial V}{\partial y}, & \frac{dy}{d\tau} &= -\varepsilon \frac{\partial V}{\partial x}. \end{aligned} \tag{6}$$

Here

$$\varepsilon = \sqrt{\mu}, \quad V(x, y, \varphi) = W(x, y, 1, \varphi).$$

Generally speaking, variables x, y, φ , and Φ in (6) vary with different rates:

$$\frac{d\varphi}{d\tau}, \frac{d\Phi}{d\tau} \sim 1, \quad \frac{dx}{d\tau}, \frac{dy}{d\tau} \sim \varepsilon.$$

Taking into account this separation of variables into fast and slow ones, we shall call the system (6) the “slow-fast” system (or SF-system). The “fast” subsystem consists of the equations for the variables φ, Φ . The “slow” subsystem describes the behavior of the variables x, y .

SF-system (6) is a Hamiltonian one, whose symplectic structure is defined by the differential form

$$\Psi = \varepsilon^{-1}dy \wedge dx + d\Phi \wedge d\varphi.$$

The corresponding Hamiltonian is

$$\mathcal{E} = \frac{3\Phi^2}{2} + V(x, y, \varphi). \tag{7}$$

2.3 Properties of the function V and related asteroid dynamics

As ε tends to zero, the resonance zone \mathcal{Z}_{res} becomes smaller, whereas the time scale of the resonance phase variations increases as ε^{-1} (in the initial units of time). The behavior of the variables φ, Φ on this time scale can be described approximately by 1DOF Hamiltonian system

$$\frac{d\varphi}{d\tau} = 3\Phi, \quad \frac{d\Phi}{d\tau} = -\frac{\partial V}{\partial \varphi}, \tag{8}$$

where x, y are considered as fixed parameters (this approximation evidently corresponds to the formal limit $\varepsilon = 0$ in (6)).

The properties of the solutions to the system (8) are determined by the function $V(x, y, \varphi)$ properties. Figure 1 presents the graphs of this function for different values of x, y . Thick blue lines in Fig. 1 characterize variations of the resonance phase φ in solutions to the system (8) with corresponding values of the Hamiltonian \mathcal{E} . The abbreviations QS, HS, and $T_{L,T}$ near the horizontal lines specify the type of the secular evolution demonstrated by the asteroid in associated motions. If $x \neq \sqrt{2(1 - \sqrt{1 - e'^2})}$ and $y \neq 0$ (i.e., $e \neq e', \varpi \neq 0$), then in the interval $[0, 2\pi]$ the function $V(x, y, \varphi)$ has two singular points $\varphi = \varphi_{SL}(x, y)$ and $\varphi = \varphi_{ST}(x, y)$ ($\varphi_{SL}(x, y) < \varphi_{ST}(x, y)$). If $x = \sqrt{2(1 - \sqrt{1 - e'^2})}$ and $y = 0$ ($e = e', \varpi = 0$), then $V(x, y, \varphi) \rightarrow +\infty$ at $\varphi \rightarrow 0(\text{mod}2\pi)$. The singular points correspond to the motions of the asteroid ending up with its collision with the planet.

Unlike the upper two graphs in Fig. 1, the lower graph of $V(x, y, \varphi)$ does not have a bounded local maximum. Figure 2 provides the examples of the set $\Lambda(e')$, consisting of the elements x, y , for which —given the values of e' — the function $V(x, y, \varphi)$ has a bounded maximum (as a function of φ). The value of the resonance phase, which provides it, is denoted by $\varphi^*(x, y)$, assuming that $\varphi^*(x, y) \in (\varphi_{SL}(x, y), \varphi_{ST}(x, y))$. From the symmetry, inherent in the system, it follows that

$$V(x, y, \varphi) = V(x, -y, 2\pi - \varphi) \tag{9}$$

and consequently

$$\varphi^*(x, 0) = \pi.$$

For $(x, y) \in \Lambda(e')$ the values of φ , for which $V(x, y, \varphi)$ has a minimum in the intervals $(\varphi_{SL}(x, y), \varphi^*(x, y))$ and $(\varphi^*(x, y), \varphi_{ST}(x, y))$, are denoted by $\varphi_{*L}(x, y)$ and $\varphi_{*T}(x, y)$, respectively.

If the eccentricities of the asteroid and the planet orbits are small, the following approximate formula can be applied:

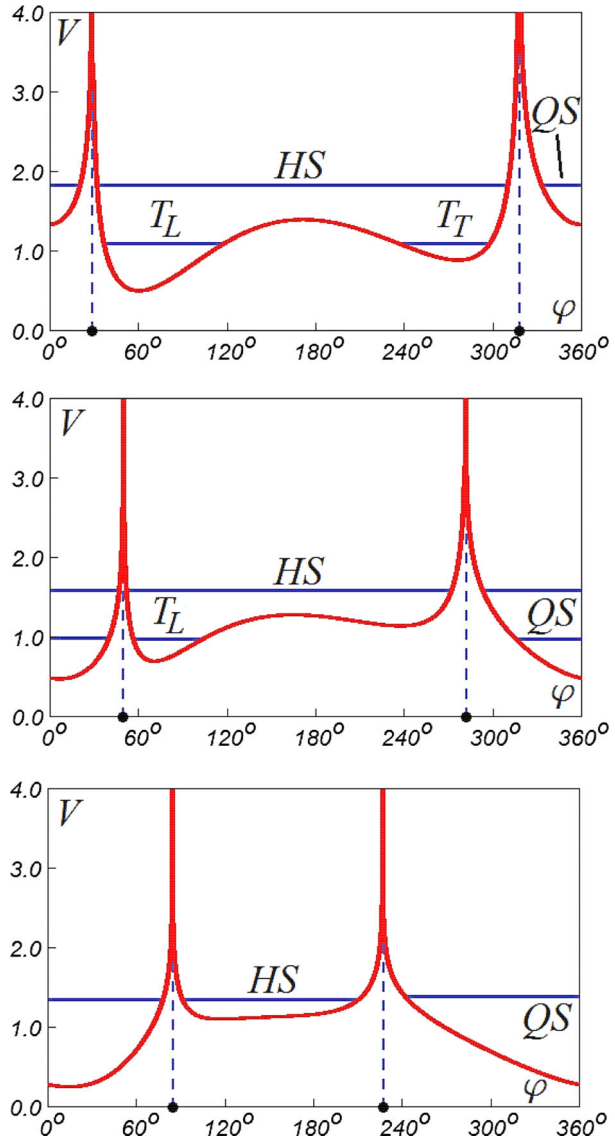
$$V(x, y, \varphi) \approx V_0(\varphi) + V_1(x, y, \varphi). \tag{10}$$

Here $\varphi \in [c_*, 2\pi - c_*]$, c_* is a positive constant, satisfying the condition $\max\{e, e'\} \ll c_* \ll 1$,

$$\begin{aligned} V_0(\varphi) &= \frac{1}{\sqrt{2(1 - \cos \varphi)}} - \cos \varphi, \\ V_1(x, y, \varphi) &= (x^2 + y^2 + e'^2)g_0(\varphi) + e'(xg_1(\varphi) + yg_2(\varphi)), \\ g_0(\varphi) &= \frac{\cos \varphi}{2} + \frac{9 - 5 \cos^2 \varphi - 4 \cos \varphi}{4(2 - 2 \cos \varphi)^{5/2}}, \\ g_1(\varphi) &= 1 - 2 \cos^2 \varphi + \frac{\cos^3 \varphi + 8 \cos^2 \varphi - 5 \cos \varphi - 4}{2(2 - 2 \cos \varphi)^{5/2}}, \\ g_2(\varphi) &= 2 \cos \varphi \sin \varphi + \frac{\sin \varphi(9 - \cos^2 \varphi - 8 \cos \varphi)}{2(2 - 2 \cos \varphi)^{5/2}}. \end{aligned}$$

The approximate expression (10) for the disturbing function is actually a special case of a more general formula obtained by Morais (1999), although the expression presented in Morais (1999) lacks the term of the order e'^2 .

Fig. 1 Behavior of the function V with fixed x, y . Upper panel: $x = 0.15176, y = -0.26285$ ($e = 0.3, \varpi = 60^\circ$). Middle panel: $x = 0.31623, y = -0.54772$ ($e = 0.6, \varpi = 60^\circ$). Lower panel: $x = 0.53100, y = -0.91987$ ($e = 0.9, \varpi = 60^\circ$). In all cases, the eccentricity of the planet $e' = 0.3$



Following (Sidorenko 2006; Sidorenko et al. 2014) we introduce the auxiliary functions

$$H^*(x, y) = V(x, y, \varphi^*(x, y)), \quad H_* = \min_{\varphi \in (\varphi_{SL}(x, y), \varphi_{ST}(x, y))} V(x, y, \varphi),$$

$$H_{**} = \max\{V(x, y, \varphi_{*L}(x, y)), V(x, y, \varphi_{*T}(x, y))\}.$$

The auxiliary functions $H^*(x, y)$ and H_{**} are defined on $\Lambda(e')$, and the function $H_*(x, y)$ is defined on the disk $\mathcal{D} = \{x^2 + y^2 < 1\}$. Figure 3 presents sample graphs of the functions $H^*(x, y), H_*(x, y)$, and $H_{**}(x, y)$ for $e' = 0.3$.

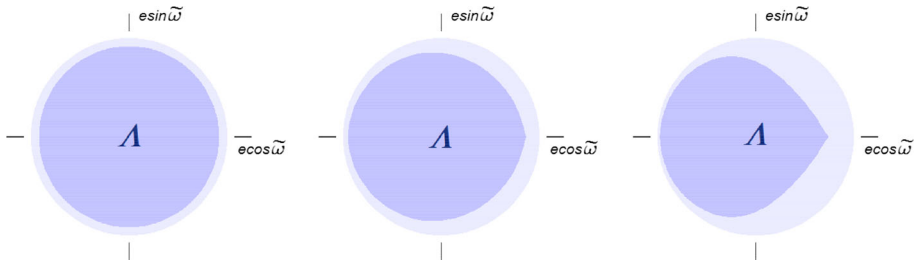


Fig. 2 The location of $\Delta(e')$ (drawn in deep blue) in the set of possible values of slow variables for different values of eccentricity of the planet. Left panel: $e' = 0$. Middle panel: $e' = 0.3$. Right panel: $e' = 0.6$. We find it more clear to present diagrams and phase portraits in terms of the variables e, ϖ . To relate these variables with the variables x, y we use the formulae (2) with $\mu = 0$, which is in accordance with the accuracy of our analysis

If $e' \neq 0$, then the function $H^*(x, y)$ has a global maximum when

$$x^* = -\sqrt{2(1 - \sqrt{1 - e'^2})}, \quad y^* = 0.$$

Taking into account the relations

$$\frac{\partial H^*}{\partial x} = \frac{\partial V}{\partial x} \Big|_{\varphi=\varphi^*(x,y)}, \quad \frac{\partial H^*}{\partial y} = \frac{\partial V}{\partial y} \Big|_{\varphi=\varphi^*(x,y)}, \quad \frac{\partial V}{\partial \varphi} \Big|_{\varphi=\varphi^*(x,y)} = 0,$$

we conclude that SF-system (6) has a stationary solution

$$x \equiv x^*, \quad y \equiv 0, \quad \varphi \equiv \pi, \quad \Phi \equiv 0.$$

This solution corresponds to the asteroid being at the collinear libration point L_3 .

The function $H_*(x, y)$ has a minimum when

$$x_*^\pm = \pm \sqrt{\frac{3(1 - \sqrt{1 - e'^2})}{2}}, \quad y_* = \sqrt{\frac{3(1 - \sqrt{1 - e'^2})}{2}}.$$

The corresponding stationary solutions to (6)

$$x \equiv x_*^\pm, \quad y \equiv y_*, \quad \varphi \equiv \pm \frac{\pi}{3}, \quad \Phi \equiv 0,$$

describe the stay of the asteroid at “leading” and “trailing” libration points, respectively.

If the planet’s eccentricity is sufficiently small, then the formula (10) allows obtaining an approximate expression for the function $H^*(x, y)$ in a neighborhood of the origin $(0, 0)$:

$$H^*(x, y) \approx \xi^* + (x^2 + y^2 + e'^2)g_0(\pi) + e'xg_1(\pi) = \xi^* - \frac{7}{16} [(x + e')^2 + y^2]. \quad (11)$$

Here

$$\xi^* = V_0(\pi) = \frac{3}{2}.$$

It is worth noting that $e' \ll 1$ entails

$$x^* \approx -e'.$$

Fig. 3 Graphs of the functions H^* , H_* , and H_{**} ($e' = 0.3$)

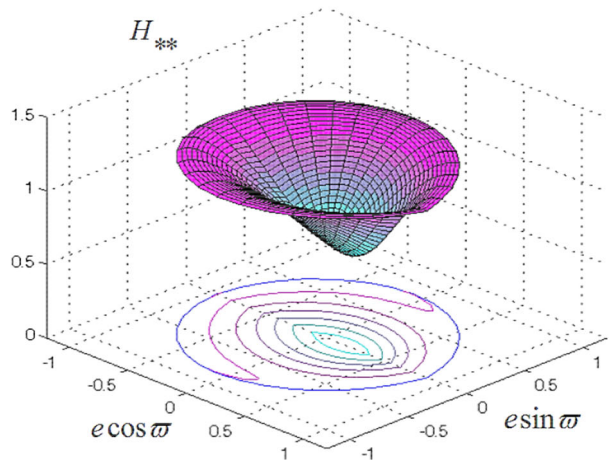
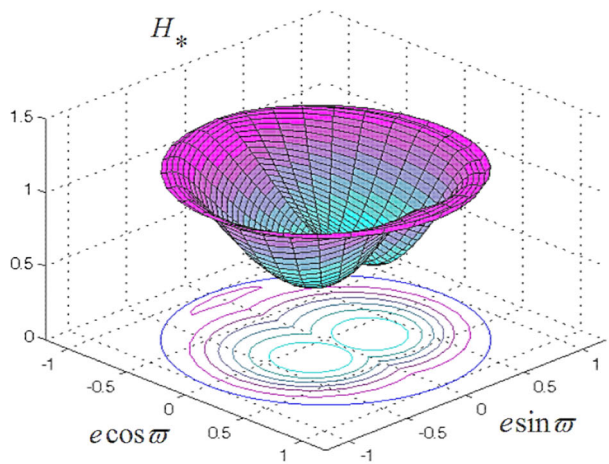
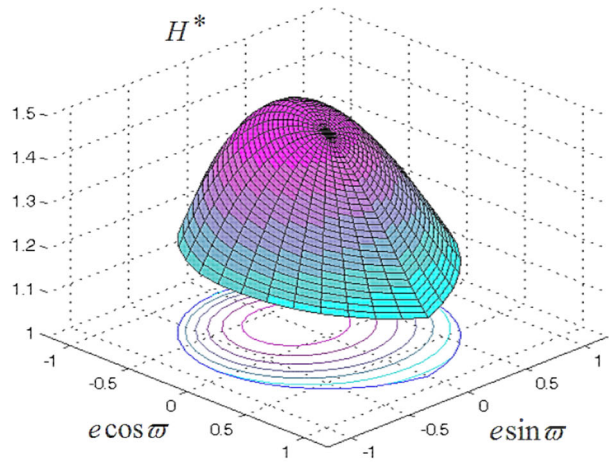
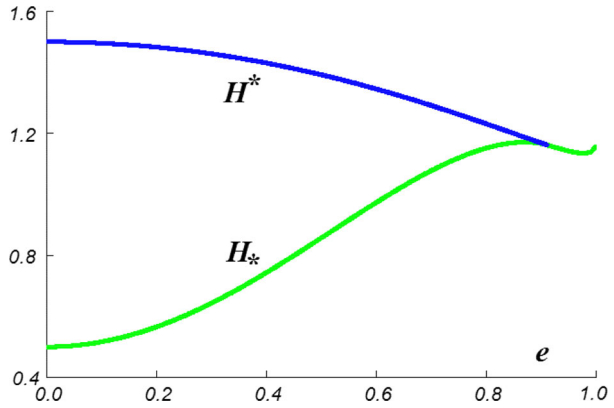


Fig. 4 Graphs of the functions H^* and H_* in for $e' = 0$



For $e' = 0$ the value of the auxiliary function at a point (x, y) is determined by the distance from this point to the origin:

$$H^*(x, y) = H^*(r), \quad H_*(x, y) = H_*(r), \quad H_{**}(x, y) = H_{**}(r),$$

where $r = \sqrt{x^2 + y^2}$. Similarly, the function V depends in this case on r and φ ; instead of (9) we have

$$V(r, \varphi) = V(r, 2\pi - \varphi). \tag{12}$$

In the resonance zone \mathcal{Z}_{res} with accuracy of order ε

$$e = \sqrt{1 - \left(1 - \frac{r^2}{2}\right)^2}$$

and, consequently, at $e' = 0$ the auxiliary functions actually depend on the value of the asteroid’s eccentricity e . In particular, the numerically obtained relation

$$e < e_b, \quad e_b = 0.91755 \dots$$

specifies the set $\Lambda(0)$ where the function H^* is defined. The symmetry (12) implies that for $e \uparrow e_b$, we have

$$\varphi_{*L}, \varphi_{*T} \rightarrow \varphi^* = \pi. \tag{13}$$

The graphs of the functions $H^*(e), H_*(e)$ are shown in Fig. 4. It follows from (13) that

$$H^*(e) \rightarrow H_*(e)$$

at $e \uparrow e_b$. The graph of the third auxiliary function is not given, since for $e' = 0$

$$H_{**} = H_*$$

for all $(x, y) \in \Lambda(0)$.

2.4 The solutions to the fast subsystem at $\varepsilon = 0$

Let

$$\varphi(\tau, x, y, \xi), \quad \Phi(\tau, x, y, \xi) \tag{14}$$

denote a solution to Eq. (8), satisfying the condition

$$\mathcal{E}(\varphi(\tau, x, y, \xi), \Phi(\tau, x, y, \xi), x, y) = \xi.$$

In general, the angle φ in the solution (14) oscillates with a period $T(x, y, \xi)$.

If $(x, y) \in \Lambda(e')$, then for $\xi \in (H_{**}(x, y), H^*(x, y))$ at the level set $\mathcal{E} = \xi$ there are two periodic solutions corresponding to motions in T_L -orbit ($\varphi_{SL} < \varphi < \varphi^*(x, y)$) and T_T -orbit ($\varphi^* < \varphi < \varphi_{ST}(x, y)$), respectively. In other cases a periodic solution, in which $\varphi \in (\varphi_{SL}(x, y), \varphi_{ST}(x, y))$, is either unique or does not exist at all.

We shall associate with the solution (14) the action integral

$$I(x, y, \xi) = \frac{3}{2\pi} \int_0^{T(x, y, \xi)} \Phi^2(\tau, x, y, \xi) d\tau. \tag{15}$$

When $\varepsilon \neq 0$, the variables $x(\tau), y(\tau)$ can be regarded as slowly varying parameters of the fast subsystem. Therefore, the relation (15) defines the adiabatic invariant (AI) of the SF-system (6).

2.5 Averaging along the fast subsystem solutions

Averaging along (14) the right-hand sides of the equations for the slow variables x, y in the system (6) yields the evolutionary equations

$$\frac{dx}{d\tau} = \varepsilon \left\langle \frac{\partial V}{\partial y} \right\rangle, \quad \frac{dy}{d\tau} = -\varepsilon \left\langle \frac{\partial V}{\partial x} \right\rangle, \tag{16}$$

where

$$\left\langle \frac{\partial V}{\partial \xi} \right\rangle = \frac{1}{T(x, y, \xi)} \int_0^{T(x, y, \xi)} \frac{\partial V}{\partial \xi}(x, y, \varphi(\tau, x, y, \xi)) d\tau. \tag{17}$$

Applying the averaging procedure (17) it is necessary to take into account that the solution (14), lying at the chosen level $\mathcal{E} = \xi$, can be aperiodic. (In other words, it can correspond to the separatrix on the phase portrait of the fast subsystem.) To distinguish these situations, we introduce the set

$$\Gamma(\xi) = \{(x, y) \in \Lambda(e'), H^*(x, y) = \xi\}.$$

The set $\Gamma(\xi)$ consists of points with such coordinates (x, y) that there exists an aperiodic solution (14)–(8). Similarly to Wisdom (1985) and Neishtadt (1987a), this set is further referred to as the uncertainty curve. A detailed discussion of the dynamical effects is possible when the projection of the phase point

$$\mathbf{z}(t) = (x(t), y(t), L(t), \varphi(t))^T$$

onto the plane x, y approaches the uncertainty curve $\Gamma(\xi)$ given in Neishtadt (1987b), Neishtadt and Sidorenko (2004) and Sidorenko et al. (2014).

For simplicity, we limit our analysis to the case when the uncertainty curve $\Gamma(\xi)$ is an oval. This is the case when $\xi \in (\xi^{**}, \xi^*)$, where

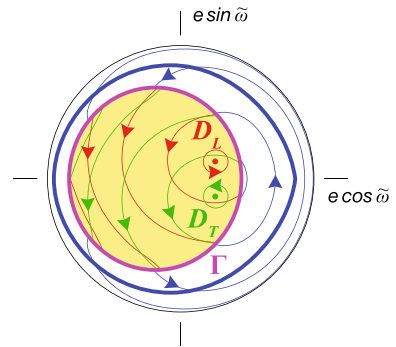
$$\xi^{**} = \max_{(x, y) \in \partial \Lambda} \overline{H}^*(x, y),$$

$\overline{H}^*(x, y)$ denotes the continuous extension of the function $H^*(x, y)$ to the boundary of $\Lambda(e')$.

It follows from the formula (11), under the condition

$$0 < \xi^* - \xi \ll 1$$

Fig. 5 Phase portrait of the system (16) for $\xi = 1.3$, $e' = 0.3$



and for small values of the planet eccentricity the uncertainty curve is close to a circle of radius

$$R(\xi) = 4\sqrt{\frac{\xi^* - \xi}{7}}$$

with the center at the point $(-e', 0)$.

Let $D(\xi)$ be a set of points lying inside the curve $\Gamma(\xi)$. If $(x, y) \in D(\xi)$, then there are two periodic solutions on the level $\mathcal{E} = \xi$, corresponding to the asteroid’s motion in T_L - and T_T -orbits. Averaging (6) along these solutions yields, generally speaking, a different result. Thus, in the region $D(\xi)$ the evolutionary Eqs. (16) have two families of phase trajectories describing the secular evolution of T_L -orbits and T_T -orbits, respectively. Examples will be given in the next Section.

3 Secular evolution and transitions between different types of the orbital motion

Numerical investigation has shown that at $\xi = \xi_b \approx \xi^* - \frac{7}{4}$, a bifurcation occurs leading to a change in the number of fixed points of the system (16). For this reason, we shall separately consider the cases

$$\xi \in (\xi^{**}, \xi_b) \tag{18}$$

and

$$\xi \in (\xi_b, \xi^*). \tag{19}$$

3.1 Secular evolution for $\xi \in (\xi^{**}, \xi_b)$

Figure 5 presents a typical phase portrait of the system (16), when ξ satisfies the condition (18). To obtain this and other phase portraits, we integrated Eq. (16) numerically. Trajectories approaching the uncertainty curve are formally glued with trajectories starting on this curve. At some points of the curve $\Gamma(\xi)$ two trajectories start simultaneously. It means that the projection of a phase point $\mathbf{z}(\mathbf{t})$ onto the plane x, y can leave the neighborhood of $\Gamma(\xi)$ along any of these trajectories. This phenomenon allows a probabilistic interpretation (Sect. 4). A more detailed discussion of a similar situation can be found in Sidorenko et al. (2014), where temporal transitions to quasi-satellite orbits are considered under the scope of 3D RC3BP.

Red and green trajectories in Fig. 5 characterize the secular evolution in the cases of the asteroid’s motion in T_L -orbit and T_T -orbit, respectively. Up to the directions of the arrows, these families of the trajectories are symmetric with respect to the horizontal axis. For $(x, y) \in \Lambda(\xi')$, the blue trajectories correspond to the motion in HS-orbit, whereas outside of $\Lambda(e')$ the usual classification of orbits at 1 : 1 MMR almost loses its sense.

There are eight fixed points on the described phase portrait. The fixed points A and B lie outside the region $D(\xi)$. The points C_L, D_L , and E_L are the fixed points of evolutionary Eq. (16) averaged along T_L -orbits. Similarly, the points C_T, D_T , and E_T are the fixed points of (16) averaged along T_T -orbits. In Fig. 5, only the fixed points D_L and D_T are shown, since the remaining points are very close to the curve $\Gamma(\xi)$. The enlarged fragments of the phase portrait in the vicinity of the points A, B, C_T , and E_T are presented in Fig. 6. The behavior of the phase trajectories in the vicinity of the fixed points C_L and E_L is similar to the fragments with the points C_T and E_T , respectively, up to the reflection with respect to the horizontal axis, followed by a change of colors and directions of the arrows.

Figure 6a shows the behavior of phase trajectories in the vicinity of the unstable fixed point B lying outside $D(\xi)$. The point $R \in \Gamma(\xi)$ is the limit point for a family of trajectories in the curvilinear triangle, whose sides are formed by the separatrices of the saddle point B and the segment of the uncertainty curve $\Gamma(\xi)$.

Figure 6b demonstrates the behavior of trajectories in the vicinity of the stable fixed point A also lying outside the region $D(\xi)$. It can be seen, that as a limit, the family of trajectories, encircling this point, contains a trajectory tangent to the curve $\Gamma(\xi)$ at the point Q .

Figure 6c shows a vicinity of the fixed point C_T of the averaged equations describing the evolution of T_T -orbits. The family of trajectories encircling C_T includes as a limit a trajectory tangent to $\Gamma(\xi)$ at the point R_T .

Figure 6d illustrates the behavior of the phase trajectories in the vicinity of the unstable fixed point E_T of Eq. (16) averaged along the T_T -orbits. The point $Q_T \in \Gamma(\xi)$ is the limit point for a family of trajectories in curvilinear triangle formed by the separatrices of the saddle point E_T and the segment of the uncertainty curve $\Gamma(\xi)$.

The properties of the stable stationary solutions A, C_L , and C_T have been given a closer look in Morais (1999) for different values of a parameter that is actually equivalent to the parameter ξ .

The points Q, Q_L, Q_T, R, R_L, R_T generate the partition of the curve $\Gamma(\xi)$ into segments with different asteroid’s motion transformations (Fig. 7). All possible scenarios are listed in Table 1. As an example, Fig. 8 shows the results of numerical integration of non-averaged motion equations, demonstrating the transition $T_T \rightarrow T_L$ in the vicinity of the segment $R_T R$. It should not come as a surprise that the resonance phase φ in Fig. 8 does not oscillate around 300° for trailing orbit and around 60° for leading orbit. Oscillations around these values take place when $e \approx e', \varpi \approx 300^\circ$ or $\varpi \approx 60^\circ$, respectively (i.e., when the configuration of the system “Sun + planet + asteroid” is close to rotating and pulsating equilateral triangle). As shown in Fig. 1, in other cases the location of the minima of the function V in the interval $(\varphi_{SL}, \varphi_{ST})$ can be elsewhere.

If the uncertainty curve encircles the origin $(0, 0)$ in the plane of the slow variables, then the longitude of periaapsis ϖ can be used as a parameter that determines the position of the phase point on $\Gamma(\xi)$:

$$\varpi = \begin{cases} 2\pi - \arccos \frac{x}{\sqrt{x^2+y^2}}, & y \geq 0; \\ \arccos \frac{x}{\sqrt{x^2+y^2}}, & y < 0. \end{cases}$$

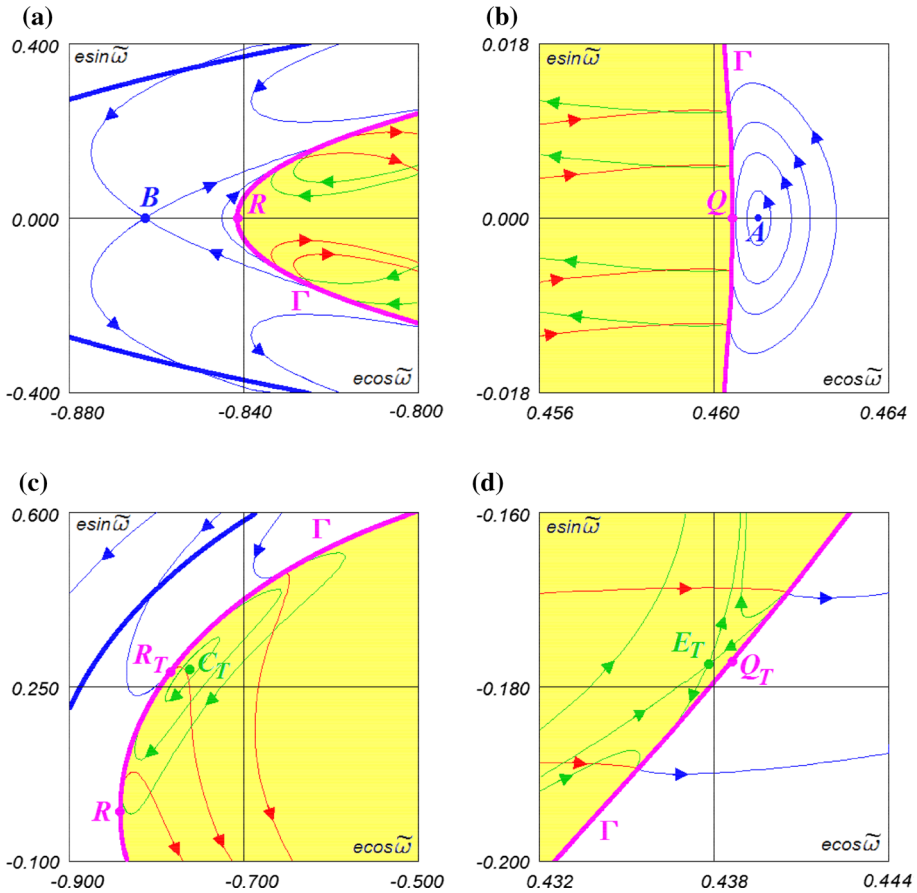


Fig. 6 Behavior of the phase trajectories in the vicinity of the fixed points ($\xi = 1.3, e' = 0.3$)

Table 1 Transformations of the motion regimes in the vicinity of the uncertainty curve

Segment	$Q Q_L$	$Q_L R_T$	$R_T R$	$R R_L$	$R_L Q_T$	$Q_T Q$
Possible transitions	$\begin{matrix} HS \\ \searrow \\ T_T \\ \nearrow \\ T_L \end{matrix}$	$\begin{matrix} HS \\ \nearrow \\ T_L \\ \searrow \\ T_T \end{matrix}$	$\begin{matrix} HS \\ \searrow \\ T_L \\ \nearrow \\ T_T \end{matrix}$	$\begin{matrix} T_T \\ \nearrow \\ HS \\ \searrow \\ T_L \end{matrix}$	$\begin{matrix} T_L \\ \searrow \\ HS \\ \nearrow \\ T_T \end{matrix}$	$\begin{matrix} T_L \\ \nearrow \\ HS \\ \searrow \\ T_T \end{matrix}$

Numerical studies did not reveal any other motion transformations in the vicinity of $\Gamma(\xi)$ for $\xi \in (\xi^{**}, \xi^*)$. The value of ξ affects only the position of points Q, Q_L, Q_T, R, R_L, R_T on the uncertainty curve and the position of the uncertainty curve in the plane of the slow variables

The phase flow of the averaged equations generates a map $\Gamma \rightarrow \Gamma$. For motion in T -orbit, it is easy to establish a correspondence between the initial value of ϖ (i.e., just after the transition to this orbit) and its value, when the transition to another orbital regime takes place. An example is presented in Fig. 9. It is noteworthy that this correspondence is not uniquely defined: For some “input” values of the longitude of periapsis ϖ_{in} , the next approach to the curve $\Gamma(\xi)$ is possible with two different values ϖ_{fin} .

Fig. 7 Partition of the curve $\Gamma(\xi)$ into segments with different motion transformations. The position of the points Q, Q_L, Q_T, R, R_L, R_T is determined by the properties of some families of phase trajectories described in Sect. 3.1

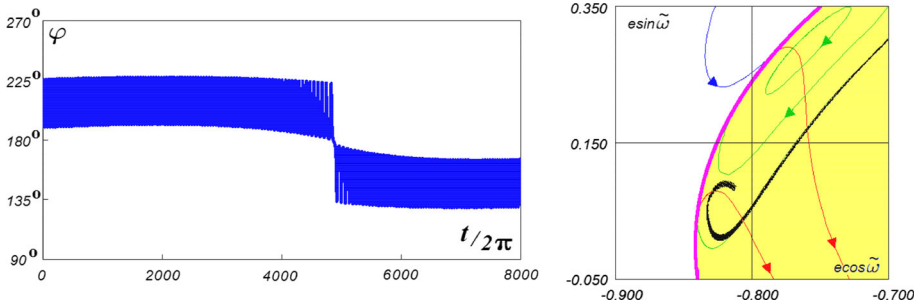
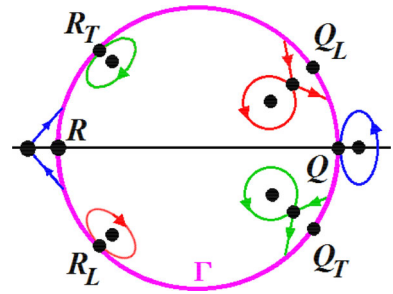
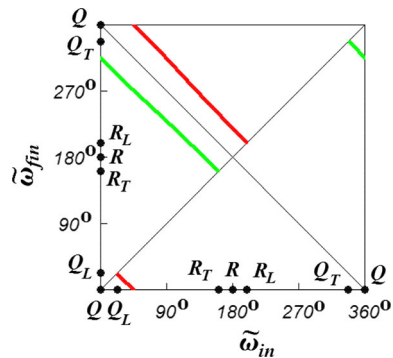


Fig. 8 An example of a transition $T_T \rightarrow T_L$ obtained by numerical integration of non-averaged equations of motion ($\mu = 0.0001, e' = 0.3$). The black curve on the right panel characterizes the evolution of the slow variables in this solution

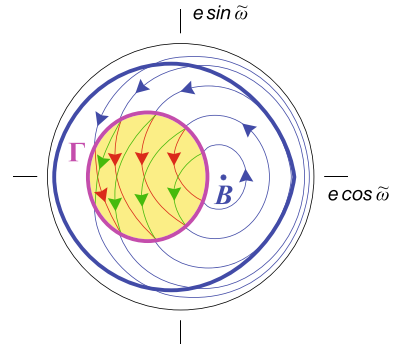
Fig. 9 A correspondence between the value of the longitude of periaapsis just after the transition and its value just before the next transition for motion in T -orbit ($\xi = 1.3, e' = 0.3$). Red and green curves correspond to T_L -regime and T_T -regime, respectively



3.2 Secular evolution for $\xi \in (\xi_b, \xi^*)$

A typical phase portrait of the system (16) for $\xi \in (\xi_b, \xi^*)$ is shown in Fig. 10. Its main difference from the phase portrait in Fig. 5 is the absence of the fixed points $D_{L,T}$ and $E_{L,T}$. Nevertheless, the pairwise merging of these points at $\xi = \xi_b$ does not affect the behavior of the phase trajectories in the vicinity of the uncertainty curve. And, consequently, there are no qualitative changes in the partition of $\Gamma(\xi)$ into segments with different motion transformations.

Fig. 10 Phase portrait of the system (16) at $\xi = 1.4$, $e' = 0.3$



4 The transitions between different types of the co-orbital motions: probabilistic characteristics

Figure 11 presents the results of numerical integration of non-averaged motion equations demonstrating the transition to different orbital regimes when the projection of the phase point $\mathbf{z}(t)$ onto the plane of the slow variables intersects the uncertainty curve virtually in the same place. The fact that the qualitatively different variants of the secular evolution can be realized, when the phase points leave the vicinity of $\Gamma(\xi)$, means faster “chaotization” of the dynamics of the system in comparison with the case when the “scattering” of the trajectories in the vicinity of $\Gamma(\xi)$ is associated only with a violation of adiabaticity (as, for example, in Neishtadt (1987a, b) and Wisdom (1985)).

In case of a strong mixing of the initial conditions corresponding to different dynamical regimes, the probabilistic estimates of the possible motion transformations become meaningful. Indeed, even a small uncertainty in the initial conditions does not allow to predict uniquely the qualitative character of the motion over long time intervals. Not being rigorous enough, we define the probability of a certain motion regime as the relative measure of the set of initial conditions leading to this regime in the sufficiently small region of the phase space. Strict definition is given in Arnold (1963) and Neishtadt (1987b).

To obtain the transition probabilities, we calculate the values of the auxiliary quantities introduced in Neishtadt (1987b) and Artemyev et al. (2013):

$$\Theta_{L,T} = \int_{-\infty}^{+\infty} \left(\frac{\partial H^*}{\partial x} \frac{\partial V}{\partial y} - \frac{\partial H^*}{\partial y} \frac{\partial V}{\partial x} \right)_{\varphi_{L,T}^s(\tau, x, y)} d\tau.$$

Here $\varphi_{L,T}^s(\tau, x, y)$ denotes aperiodic solutions of the fast subsystem lying on the critical level $\mathcal{E} = H^*(x, y)$.

The quantities Θ_L and Θ_T are time derivatives of the area of the regions bounded by the separatrices on the phase portraits of the fast subsystem, when the slow variables evolve according to Eq. (16).

If the projection of the phase point $\mathbf{z}(t)$ onto the plane of slow variables approaches the uncertainty curve $\Gamma(\xi)$, then the probabilities of the subsequent motion regimes are given by formulae by Artemyev et al. (2013):

$$P_{L,T} = \frac{\hat{\Theta}_{L,T}}{\hat{\Theta}_L + \hat{\Theta}_T + \hat{\Theta}}, \quad P_{HS} = 1 - P_L - P_T, \tag{20}$$

where $\hat{\Theta}_{L,T} = \max(\Theta_{L,T}, 0)$, $\hat{\Theta} = \max(-\Theta_L - \Theta_T, 0)$.

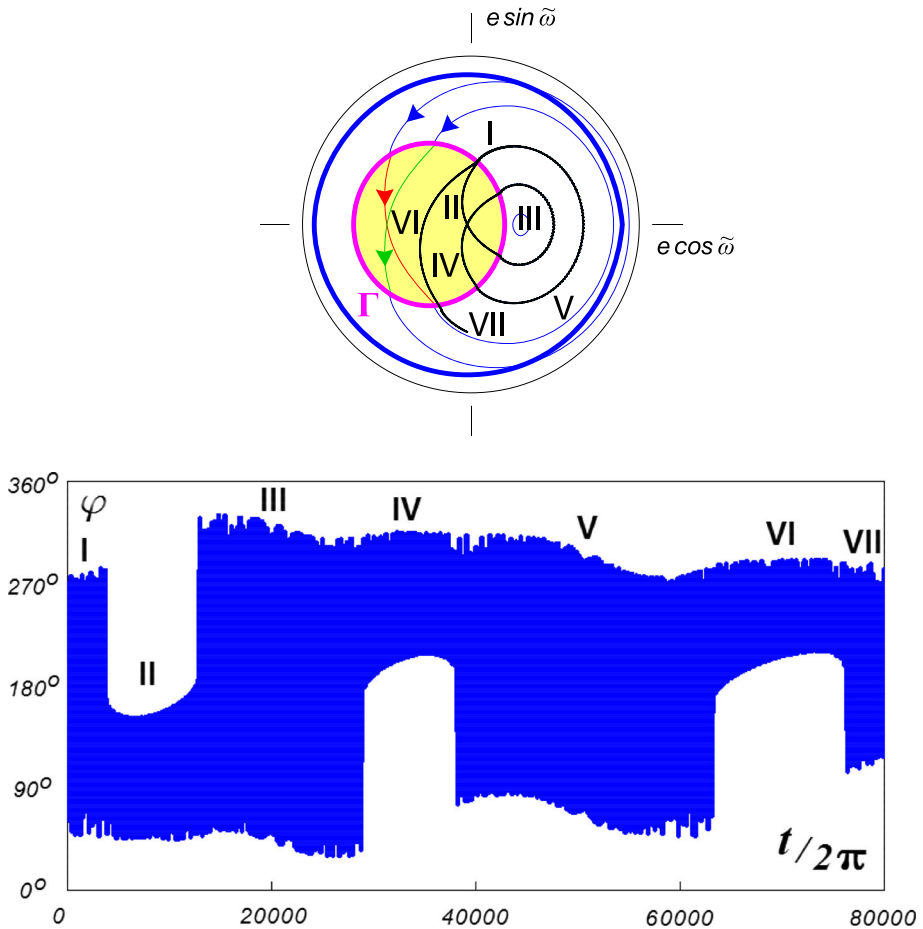


Fig. 11 Example of the motion with transformations of resonance regimes on the uncertainty curve Γ . Black curve on the top panel characterizes the evolution of the slow variables in this solution of the non-averaged equations ($\mu = 0.00002$, $\xi = 1.4$, $e' = 0.3$). Segments I and V of the presented solution practically coincide (up to a quasi-random component of AI variation in the vicinity of Γ) and end at close points of the uncertainty curve

Figure 12 provides an example of the probability distribution of various transitions along the curve $\Gamma(\xi)$. Calculations were carried out using the formulae (20) for the case $\xi = 1.3$, $e' = 0.3$. Although the comprehensive investigation of the transitions probabilities was beyond our goals, we carried out the similar calculations for some other values of ξ for which the uncertainty curve $\Gamma(\xi)$ encircles the origin $(0, 0)$ on the plane of the slow variables (more precisely, for $\xi \in (1.24, 1.45)$, $e' = 0.3$). The results show no significant qualitative difference in the distribution of probabilities.

Having obtained more or less comparable probabilities for transitions $HS \rightarrow T_L$ and $HS \rightarrow T_T$, we can suppose that the observed predominance of the T_L -orbits among the Jupiter Trojan asteroids (Emery et al. 2015) is caused by some factors that are not present in our model.

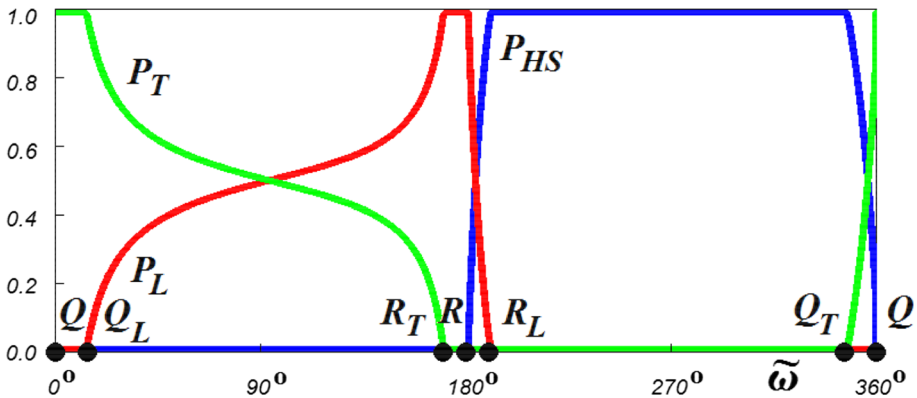


Fig. 12 The probabilities of transitions to different regimes of co-orbital motion when the projection of the phase point $\mathbf{z}(t)$ onto the plane of the slow variables approaching the curve Γ ($\xi = 1.3$, $e' = 0.3$). The probabilities of further motion in T_L -orbit and T_T -orbit are indicated by red and green curves, respectively, blue curve corresponds to the motion in HS-orbit

5 Conclusion

The goal of this paper is to present a simple, but robust mechanism of the motion transformations are 1:1 MMR as a result of which leading Trojan asteroids become trailing ones and vice versa. To reveal such mechanism, we applied a semianalytical approach based on ideas of “adiabatic approximation” introduced by J. Wisdom in his studies of resonant phenomena in the asteroid belt. The remarkable feature of this approach is the absence of any restrictions on the studied resonance motion (in particular, it is not limited to the case of small eccentricities and inclinations).

For clarity, we plotted the phase portraits characterizing the secular effects in the orbital motion of an asteroid at 1:1 MMR. The transformation of the motion takes place when the phase point reaches the so-called uncertainty curve on the phase portrait. Analyzing different transformations, we established that the transfers between populations of leading and trailing Trojans are indeed possible under the scope of planar-restricted elliptic three-body problem. We also computed the probability distributions of various transitions along the uncertainty curve.

Similar transitions between different resonance regimes occur at other MMR as well. Examples can be found in Chiang and Jordan (2002) and Ketchum et al. (2013). To describe the motion with such transitions, Ketchum et al. (2013) proposed a rather illustrative term “nodding behavior.” We consider the analysis of “nodding behavior” as a very interesting trend in the studies on MMR and hope to have contributed to its progress.

Acknowledgements The work was supported by the Presidium of the Russian Academy of Sciences (Program 7 “Experimental and theoretical studies of the objects in the Solar system and exoplanetary systems”). We are grateful to S.S. Efimov, B. Erdi, A.I. Neishtadt, and D.A. Pritykin for reading the manuscript and useful discussions. We also thank anonymous referees for all their corrections and suggestions.

References

- Arnold, V.I.: Small denominators and problems of stability of motion in classical and celestial mechanics. *Russ. Math. Surv.* **18**, 86–191 (1963)
- Arnold, V.I., Kozlov, V.V., Neishtadt, A.I.: *Mathematical Aspects of Classical and Celestial Mechanics*, 3rd edn. Springer, New York (2006)
- Artemyev, A.V., Neishtadt, A.I., Zelenyi, L.M.: Ion motion in the current sheet with sheared magnetic field—Part I: quasi-adiabatic theory. *Nonlinear Process. Geophys.* **20**, 163–178 (2013)
- Beaugè, C., Roig, F.: A semianalytical model for the motion of the Trojan asteroids: proper elements and families. *Icarus* **153**, 391–415 (2001)
- Chiang, E.I., Jordan, A.B.: On the plutinos and twotinos of the Kuiper belt. *Astron. J.* **124**, 3430–3444 (2002)
- Connors, M., Wiegert, P., Veillet, C.: Earth’s Trojan asteroid. *Nature* **475**, 481–483 (2011)
- de la Fuente Marcos, C., de la Fuente Marcos, R.: Four temporary Neptune co-orbitals: (148975) 2001 XA255, (310071) 2010 KR59, (316179) 2010 EN65, and 2012 GX17. *Astron. Astrophys.* **547**, L2 (2012)
- Dvorak, R., Lhotka, C., Zhou, L.: The orbit of 2010 TK7: possible regions of stability for other Earth Trojan asteroids. *Astron. Astrophys.* **541**, A127 (2012)
- Emery, J.P., Marzari, F., Morbidelli, A., French, L.M., Grav, T.: The complex history of Trojan asteroids. *Asteroids IV*, 203–220 (2015)
- Erdi, B.: The Trojan problem. *Celest. Mech. Dyn. Astron.* **65**, 149–164 (1997)
- Galliazzo, M.A., Schwarz, R.: The Hungaria region as a possible source of Trojans and satellites in the inner solar system. *MNRAS* **445**, 3999–4007 (2014)
- Karlssohn, O.: Transitional and temporary objects in the Jupiter Trojan area. *Astron. Astrophys.* **413**, 1153–1161 (2004)
- Ketchum, J.A., Adams, F.C., Bloch, A.M.: Mean motion resonances in exoplanet systems: an investigation into nodding behavior. *Astrophys. J.* **762**, 1–19 (2013)
- Marzari, F., Scholl, H., Murray, C., Lagerkvist, C.: Origin and evolution of Trojan asteroids. *Asteroids III*, 725–738 (2002)
- Morais, M.H.M.: A secular theory for Trojan-type motion. *Astron. Astrophys.* **350**, 318–326 (1999)
- Morais, M.H.M.: Hamiltonian formulation of the secular theory for Trojan-type motion. *Astron. Astrophys.* **369**, 677–689 (2001)
- Namouni, F., Christou, A.A., Murray, C.D.: Coorbital dynamics at large eccentricity and inclination. *Phys. Rev. Lett.* **83**, 2506–2509 (1999)
- Neishtadt, A.I.: The separation of motions in systems with rapidly rotating phase. *J. Appl. Math. Mech. USSR* **48**, 133–139 (1984)
- Neishtadt, A.I.: Jumps of the adiabatic invariant on crossing the separatrix and the origin of the 3:1 Kirkwood gap. *Soviet Phys. Dokl.* **32**, 571–573 (1987)
- Neishtadt, A.I.: On the change in the adiabatic invariant on crossing a separatrix in systems with two degrees of freedom. *J. Appl. Math. Mech. USSR* **51**, 586–592 (1987)
- Neishtadt, A.I., Sidorenko, V.V.: Wisdom system: dynamics in the adiabatic approximation. *Celest. Mech. Dyn. Astron.* **90**, 307–330 (2004)
- Nesvorný, D., Thomas, F., Ferraz-Mello, S., Morbidelli, A.: A perturbative treatment of the co-orbital motion. *Celest. Mech. Dyn. Astron.* **82**, 323–361 (2002)
- Oshima, K., Yanao, T.: Jumping mechanisms of Trojan asteroids in the planar restricted three- and four-body problems. *Celest. Mech. Dyn. Astron.* **122**, 53–74 (2015)
- Robutel, P., Souchay, J.: An introduction to the dynamics of Trojan asteroids. *Lect. Notes Phys.* **790**, 195–227 (2010)
- Schubart, J.: Long-period effects in nearly commensurable cases of the restricted three body problem. *Smithsonian Astrophys. Obs. Spec. Report* 149 (1964)
- Schwarz, R., Dvorak, R.: Trojan capture by terrestrial planets. *Celest. Mech. Dyn. Astron.* **113**, 23–34 (2012)
- Sidorenko, V.V.: Evolution of asteroid orbits at resonance 3:1 of their mean motions with Jupiter (planar problem). *Cosm. Res.* **44**, 440–455 (2006)
- Sidorenko, V.V., Neishtadt, A.I., Artemyev, A.V., Zelenyi, L.M.: Quasi-satellite orbits in the general context of dynamics in the 1:1 mean motion resonance. Perturbative treatment. *Celest. Mech. Dyn. Astron.* **120**, 131–162 (2014)
- Tsiganis, K., Dvorak, R., Pilat-Lohinger, E.: Thersites: a “jumping” Trojan? *Astron. Astrophys.* **354**, 1091–1100 (2000)
- Wisdom, J.: A perturbative treatment of motion near the 3/1 commensurability. *Icarus* **63**, 272–286 (1985)